

# Enhanced critical current density of $\text{YBa}_2\text{Cu}_3\text{O}_x$ films grown on $\text{Nd}_{1/3}\text{Eu}_{1/3}\text{Gd}_{1/3}\text{Ba}_2\text{Cu}_3\text{O}_x$ with nano-undulated surface morphology

R. L. Meng<sup>1</sup>, T. H. Johansen<sup>1,2</sup>, I. A. Rusakova<sup>1</sup>, A. Baikalov<sup>1</sup>, D. Pham<sup>1</sup>, F. Chen<sup>1</sup>, Z. Y. Zuo<sup>1</sup>, and C. W. Chu<sup>1,3,4</sup>

<sup>1</sup>*Department of Physics and Texas Center for Superconductivity,  
University of Houston, 202 Houston Science Center, Houston, Texas 77204-5002*

<sup>2</sup>*Department of Physics, University of Oslo, N-0316 Oslo, Norway*

<sup>3</sup>*Lawrence Berkeley National Laboratory, 1 Cyclotron Road, Berkeley, California 94720 and*

<sup>4</sup>*Hong Kong University of Science and Technology, Hong Kong*

(Dated: November 29, 2018)

We report a simple and easily controllable method where a nano-undulated surface morphology of  $\text{Nd}_{1/3}\text{Eu}_{1/3}\text{Gd}_{1/3}\text{Ba}_2\text{Cu}_3\text{O}_x$  (NEG) films leads to a substantial increase in the critical current density in superconducting  $\text{YBa}_2\text{Cu}_3\text{O}_x$  (YBCO) films deposited by pulsed laser deposition on such NEG layers. The enhancement is observed over a wide range of fields and temperatures. Transmission electron microscopy shows that such YBCO films possess a high density of localized areas, typically  $20 \times 20 \text{ nm}^2$  in size, where distortion of atomic planes give rotational (2 to 5°) moiré patterns. Their distribution is random and uniform, and expected to be the origin of the enhanced flux pinning. Magneto-optical imaging shows that these films have excellent macroscopic magnetic uniformity.

Practical applications of high temperature superconductor films depend crucially upon finding ways to enhance the flux pinning and thereby increasing the critical current density,  $j_c$ , especially at high magnetic fields. Recent reports have shown that pre-decoration of the substrate by a high density of nano-sized particles is an efficient way of creating large numbers of strong pinning sites in the superconducting film that subsequently is deposited on the decorated surface. The basic idea of the method is using the nano particles to create a substantial lattice mismatch or chemical poisoning so that locally the superconducting phase is prevented to form. Successful examples of this are sputtering nano-dots of Ag on a  $\text{SrTiO}_3$  (STO) substrate prior to deposition of  $(\text{Cu},\text{Ti})\text{BaSrCa}_2\text{Cu}_3\text{O}_y$ , pulsed laser deposition of nano-islands of  $\text{Y}_2\text{O}_3$  or Ag on STO and YSZ substrates, respectively, prior to deposition of  $\text{YBa}_2\text{Cu}_3\text{O}_x$  (YBCO).<sup>1,2,3</sup> In principle, the method can be extended by repeating the double deposition, as was demonstrated with alternating growth of an ultra thin layer of second-phase  $\text{YBa}_2\text{CuO}_5$  and superconducting YBCO repeated up to 200 times.<sup>4</sup>

In this work we report a new and efficient method to obtain enhanced pinning in films of YBCO. The method is based on our observation that thin films of the mixed rare earth compound  $\text{Nd}_{1/3}\text{Eu}_{1/3}\text{Gd}_{1/3}\text{Ba}_2\text{Cu}_3\text{O}_x$  (NEG) grown by laser ablation on STO substrates develop a surface morphology with densely packed and sharply separated submicron sized growth islands. We show that by using such a nano-undulated surface as a sublayer for deposition of YBCO films one obtains an increase in  $j_c$  by approximately 50%. Magneto-optical (MO) imaging studies reveal that such YBCO films have excellent uniformity, and are therefore well suited for device applications. Moreover, since the NEG sublayer itself is superconducting, the method also gives a high engineering  $j_c$ .

Targets of NEG were prepared with stoichiometric

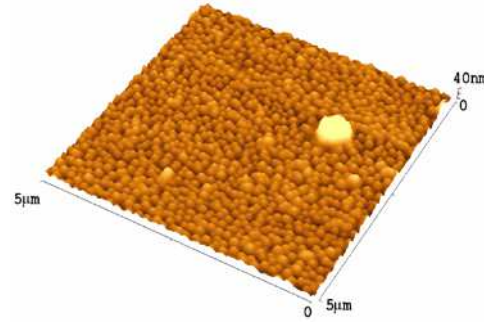


FIG. 1: AFM image of a  $5 \times 5 \mu\text{m}^2$  surface area of a NEG film deposited on STO, serving as sub-layer for subsequent deposition of a YBCO film. The NEG growth granules are nearly mono-disperse with diameter 80–100 nm and height 20–25 nm.

$\text{R}_2\text{O}_3$  ( $\text{R} = \text{Nd, Eu, Gd}$ ),  $\text{BaCO}_3$  and  $\text{CuO}$  powders sintered at 950 °C. X-ray diffraction confirmed that the target consists of pure 123 phases. The NEG films were deposited on single crystal (001) STO substrates by pulsed laser deposition. Before deposition the substrates were cleaned by heating to 900 °C for 30 minutes. The films were deposited at a temperature of 810–830 °C in a 350 mTorr oxygen atmosphere using a KrF excimer laser with RF power of 250 mJ.

Shown in Fig. 1 is the surface morphology of a typical bare NEG film observed using atomic force microscopy (AFM). This 100 nm thick film is densely packed with growth islands resulting in an undulated surface having a highly uniform and narrow distribution of peaks 15–25 nm high and 80–100 nm in diameter. This type of surface morphology is similar to that reported by Cai et al.<sup>5</sup>, and also quantitatively the AFM results are in good agreement.

In synthesizing the two-layer films the deposition of YBCO and NEG was done in the same process. We

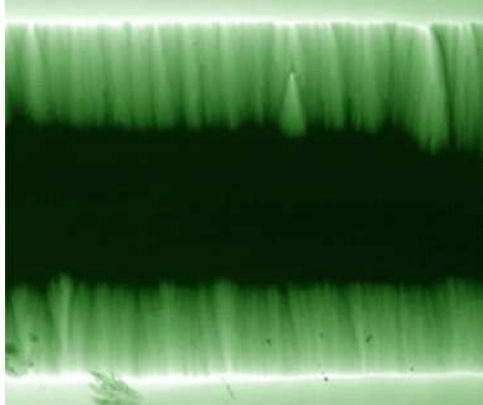


FIG. 2: MO image of flux penetration in a two-layer YBCO/NEG film. The image was recorded at 5 K in a perpendicular applied field of 45 mT, and shows the strip shaped sample in a partially penetrated state. The dark central band is the Meissner state part of the film, and the field exclusion causes the enhanced brightness seen along the film edge. The strip width is 3 mm.

found that optimal conditions for YBCO deposition is to use the same oxygen pressure and laser energy as for NEG, and lowering the deposition temperature close to 800 °C. After deposition, the films were in-situ annealed at 450–500 °C maintaining the oxygen pressure for 30 minutes, before cooling down to room temperature. No ex-situ annealing was employed. Note that the synthesis of the two films in the proper order is possible because the melting point of NEG is the higher of the two compounds.

For comparison, films of YBCO were also deposited directly on STO substrates using the same conditions. Transport measurements showed a transition temperature of 92 K for the YBCO films. The film thickness was measured using  $\alpha$ -step surface profilometry.

All samples were investigated by MO imaging using in-plane magnetized bismuth substituted iron garnet films as indicator. The setup consists of an Olympus polarizing microscope and an Oxford Microstat-He optical cryostat with a custom made coil to apply an external magnetic field. We used a fully crossed polarizer and analyzer setting, giving images where the brightness represents the magnitude of the local flux density. Shown in Fig. 2 is an MO image of a YBCO/NEG sample with layer thicknesses of 100 nm and 50 nm, respectively. The image was taken at 5 K in an applied field of  $B_a = 45$  mT. As seen directly from the image, the two-layer film has excellent uniformity in superconducting properties on the macroscopic scale. Only one defect in the upper half of the film is visible, as it creates a parabolic fan-like flux pattern starting from a point inside the strip. Since the superconducting film covers the whole substrate area, a slight edge roughness is also causing fan-like flux structures, which can be seen starting from both the upper and lower edge in the image.

TABLE I: The table shows  $j_c$  in units of  $10^7$  A/cm<sup>2</sup> for the YBCO film grown on a NEG sublayer at different temperatures. Shown is also the  $j_c$  of a reference YBCO film.

	5 K	60 K	77 K
YBCO/NEG/STO	7.2	1.8	0.46
YBCO/STO	4.7	1.2	0.24

From MO images the low-field critical current density was determined from the Bean model formula for a long thin strip,  $\mu_0 J_c = \pi B_a / \cosh^{-1}(w/a)$ . Here  $J_c$  is the sheet current (the current density integrated over the film thickness), and  $a$  and  $w$  are the width of the central flux free area and the width of the strip itself, respectively. Since these samples consist of two different superconducting layers, the sheet current has two contributions;  $J_c = j_c d + j_c^{NEG} d^{NEG}$ , where  $j_c$  and  $d$  are the critical current density and thickness of the YBCO layer, and where the second term represents the current flowing in the NEG layer. We determined  $j_c^{NEG}$  from MO images of flux penetration in bare NEG films prepared under the same deposition conditions. The current density in this layer was not very high, e.g.,  $j_c^{NEG}(5$  K) =  $0.7 \cdot 10^7$  A/cm<sup>2</sup>, but then optimizing the critical current in the NEG film was not our focus in the present work. Using the procedure described above we find for the YBCO layer alone that  $j_c = 7.1 \cdot 10^7$  A/cm<sup>2</sup> at 5 K. At higher temperatures we obtain the values listed in the Table I. Included in the table is also  $j_c$  values measured on a reference YBCO/STO sample grown under the same conditions. We find consistently that YBCO on NEG gives an enhancement in  $j_c$  of 50%–100% between 5 K and 77 K.

The field dependence of  $j_c$  was measured in the field range from zero and up to 5 T using a SQUID magnetometer. The results are plotted in Fig. 3, where full symbols show  $j_c$  of YBCO on NEG, and open symbols represent YBCO/STO. For the two-layer film  $j_c$  of the YBCO part was extracted using that in fully penetrated states the measured magnetic moment equals  $m = (j_c d + j_c^{NEG} d^{NEG}) \times$  geometrical factor, where the second factor is given by the sides of the rectangular sample used for the SQUID measurements. The results clearly show that also the field behavior of the YBCO film is largely improved by the NEG sublayer. Over the whole field range  $j_c$  is increased by 40–50% both at 5 K and 45 K. Note that the zero-field  $j_c$  obtained from the M-H loop width is slightly lower than the values obtained from MOI, which is to be expected as explained in Ref. 6.

To clarify the origin of this pinning enhancement the samples were investigated by transmission electron microscopy (TEM) using a JEOL 2000FX microscope operated at 200 kV. Cross-sectional samples were prepared by a standard procedure and ion milling was carried out with 4 keV Ar ions. Shown in Fig. 4a is a TEM bright-field image of a double layer film obtained un-

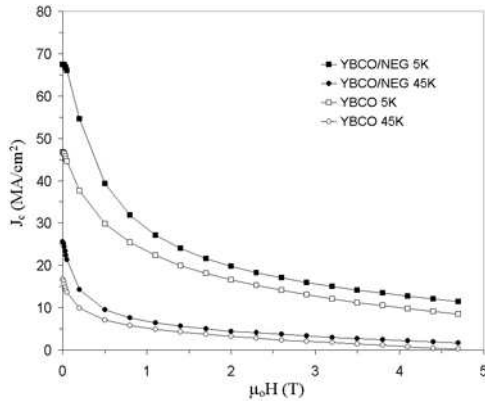


FIG. 3: Critical current density in YBCO films as a function of applied magnetic field. The solid symbols represent YBCO deposited on a NEG sub-layer, and open symbols show YBCO on the bare STO substrate.

der mass-thickness contrast image formation conditions. This type of contrast arises from incoherent (Rutherford) elastic scattering of electrons, which is a strong function of atomic number  $Z$ . The difference between the Y ions ( $Z = 39$ ) in the upper YBCO film and the much heavier ions of Nd, Eu, and Gd ( $Z = 60, 63$ , and  $64$ , respectively) in the sublayer results in a clear contrast between the two films. Their interface has a very distinct wavy appearance, which is in full quantitative agreement both in inter-peak distance and in undulation amplitude with the AFM image obtained for the bare NEG film. We conclude therefore that its surface morphology remains intact throughout the deposition of the YBCO film. Note also from the TEM image that both the NEG/STO and the YBCO/NEG interfaces are very uniform. Moreover, selected area electron diffraction (SAED) recorded from the substrate and the two layers shows that both films are very well c-axis aligned with the substrate, see Fig. 4c.

Shown in Fig. 4b is the microstructure of the double layer film obtained by conventional bright-field TEM revealing strain contrast. While the NEG/STO shows strain mainly along the interface, the YBCO layer contains numerous strained regions throughout its volume. Whereas the strain contrast at the NEG/STO interface is due to mismatch of lattice parameters, this is not the case for the YBCO/NEG interface which has nearly identical lattice constants. This strongly suggests that the strained regions inside the YBCO film stem from the interface undulation. Indeed, high resolution TEM, see Fig. 4d, reveals that in the YBCO layer strained regions start from the interface. Moreover, we find that locally the atomic planes have orientation deviations from  $2$  to  $5^\circ$  resulting in rotational moiré patterns, four of them shown by arrows. The size of the moiré pattern areas is very small, typically  $20 \times 20 \text{ nm}^2$ , and they are randomly and quite uniformly distributed. We believe that the presence of these structural defects strongly contributes to the enhancement of the flux pinning, and thereby the critical current density in such YBCO films. Additional

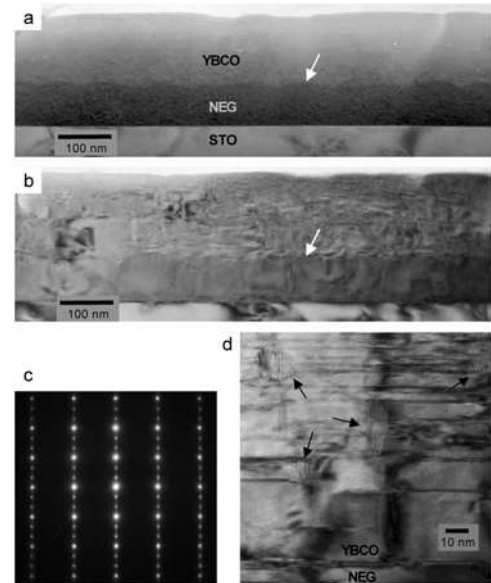


FIG. 4: (a) TEM image of the two-layer film cross section taken under mass contrast imaging conditions. (b) Conventional TEM bright-field image of the interface. In both panels, the arrow points at the undulated YBCO/NEG interface. (c) Selected area diffractogram representing the full YBCO/NEG/STO structure. (d) High resolution TEM of the YBCO layer showing several areas (see arrows) with rotational moiré patterns.

contributions can come from the high density of stacking faults, and therefore partial dislocations, as also found to be present in these films.

In conclusion, we have demonstrated that a nano-undulated surface morphology of NEG films leads to a substantial increase in the critical current density in YBCO films deposited on top of the NEG layer. The enhancement is observed over a wide range of fields and temperatures. Compared to most other methods of nanopatterning of substrates, this new method is technologically very simple, easily controllable and fast, and also economically favorable. An interesting extension of this work would be to make a periodic multilayer structure YBCO/NEG.../YBCO/NEG/STO to provide films with large total critical current. Since the NEG sublayer is also superconducting the engineering critical current of such a structure could then become very high.

### Acknowledgments

We thank Y. Y. Sun for X-ray analysis of the samples. The work in Houston is supported in part by NSF Grant No. DMR-9804325, the T. L. L. Temple Foundation, the John J. and Rebecca Moores Endowment, and the State of Texas through the Texas Center for Superconductivity at the University of Houston; and at Lawrence Berkeley Laboratory by the Director, Office of Science, Office of Basic Energy Sciences, Division of Materials Sciences

and Engineering of the U.S. Department of Energy under Contract No. DE-AC03-76SF00098. One of the authors

(THJ) is grateful to the Norwegian Research Council for financial support.

---

<sup>1</sup> A. Crisan, S. Fujiwara, J.C. Nie, A. Sundaresan and H. Ihara, *Appl. Phys. Lett.* **79**, 4547 (2001).

<sup>2</sup> K. Matsumoto et al., *Physica C* **412–414**, 1267 (2004).

<sup>3</sup> M. Ionescu, A.H. Li, Y. Zhao, H.K. Liu and A. Crisan, *J. Phys. D: Appl. Phys.* **37**, 1824 (2004)

<sup>4</sup> T. Haugan, P.N. Barnes, R. Wheeler, F. Meisenkothen and

M. Sumption, *Nature* **430**, 867 (2004).

<sup>5</sup> C. Cai, B. Holzapfel, J. Hnisch, L. Fernandez and L. Schultz, *Phys. Rev. B* **69**, 104531 (2004).

<sup>6</sup> D. V. Shantsev, Y. M. Galperin and T. H. Johansen, *Phys. Rev. B* **61**, 9699 (2000).